Published in final edited form as:
Mol Imaging Biol. 2013 April ; 15(2): 194–202. doi:10.1007/s11307-012-0576-9.

Molecular Imaging of Neuroblastoma Progression in TH-MYCN Transgenic Mice

Carmelo Quarta[1], **Erika Cantelli**[2], **Cristina Nanni**[1], **Valentina Ambrosini**[1], **Daniela D'ambrosio**[1,3], **Korinne Di Leo**[2], **Silvia Angelucci**[5], **Federico Zagni**[1,3], **Filippo Lodi**[1], **Mario Marengo**[1,3], **William A. Weiss**[4], **Andrea Pession**[2], **Roberto Tonelli**[5], and **Stefano Fanti**[1]

[1]Department of Nuclear Medicine, S. Orsola-Malpighi Hospital, University of Bologna, Bologna, Italy

[2]Pediatric Hematology–Oncology, University of Bologna, Bologna, Italy

[3]Department of Medical Physics, S. Orsola-Malpighi Hospital, Bologna, Italy

[4]University of California San Francisco, San Francisco, CA, USA

[5]Department of Pharmacology, University of Bologna, Bologna, Italy

Abstract

Purpose—TH-MYCN transgenic mice represent a valuable preclinical model of neuroblastoma. Current methods to study tumor progression in these mice are inaccurate or invasive, limiting the potential of this murine model. The aim of our study was to assess the potential of small animal positron emission tomography (SA-PET) to study neuroblastoma progression in TH-MYCN mice.

Procedure—Serial SA-PET scans using the tracer 2-deoxy-2-[^{18}F]fluoro-D-glucose (^{18}F-FDG) have been performed in TH-MYCN mice. Image analysis of tumor progression has been compared with *ex vivo* evaluation of tumor volumes and histological features.

Results—[^{18}F]FDG-SA-PET allowed to detect early staged tumors in almost 100 % of TH-MYCN mice positive for disease. Image analysis of tumor evolution reflected the modifications of the tumor volume, histological features, and malignancy during disease progression. Image analysis of TH-MYCN mice undergoing chemotherapy treatment against neuroblastoma provided information on drug-induced alterations in tumor metabolic activity.

Conclusions—These data show for the first time that [^{18}F]FDG-SA-PET is a useful tool to study neuroblastoma presence and progression in TH-MYCN transgenic mice.

Keywords

Neuroblastoma; Small animal PET; [^{18}F]FDG; TH-MYCN mice

Introduction

Neuroblastoma is the most common extracranial childhood tumor responsible for approximately 15 % of cancer-related deaths in children [1]. Neuroblastoma arises in the

Correspondence to: Carmelo Quarta; quartacarmelo@yahoo.it.
Carmelo Quarta, Erika Cantelli, Roberto Tonelli, and Stefano Fanti contributed equally to this work.

Electronic supplementary material The online version of this article (doi:10.1007/s11307-012-0576-9) contains supplementary material, which is available to authorized users.

Conflict of Interest. The authors have no conflict of interest to declare.

sympathetic nervous system, most frequently at the adrenal and medullary level [1]. Several diagnostic modalities are applied to define disease status in these patients. [(3-[^{123}I] Iodophenyl)methyl]quanidine ([^{123}I]MIBG) scintigraphy is the nuclear imaging method of choice for neuroblastoma, valuable for diagnosis, staging, and response to therapy. X-ray computed tomography (CT) or magnetic resonance imaging (MRI) is used to assess the extent of primary tumor and to detect any vascular or other vital organ involvement. MRI is the preferred modality for assessment of spinal canal cord involvement [2, 3].

In addition to these techniques, positron emission tomography/CT (PET/CT) combined imaging is emerging as a sensitive and specific tool for neuroblastoma diagnosis and staging [4–7]. 2-Deoxy-2-[^{18}F] fluoro-D-glucose ([^{18}F] FDG) is indicated in [^{123}I]MIBG-negative cases [7], and new evidence highlights the potential of experimental PET tracers such as 6-[^{18}F] fluoro-L-DOPA ([^{18}F]DOPA) and [^{68}Ga]DOTA-Tyr 3-octreotide for neuroblastoma staging [8, 9].

Mouse models of neuroblastoma provide clinically relevant tools for studying the growth and metastasis of this aggressive malignancy. Orthotopic and heterotopic xenograft mouse models have been extensively employed for preclinical testing of new therapeutic strategies against neuroblastoma. To generate these models, human neuroblastoma cell lines or neuroblastoma cells cultured from newly *ex vivo* explanted tumors are injected into recipient animals. Several variables limit the value of information obtained by these approaches. In order to avoid rejection of implanted cells, recipient animals must be immunocompromised. Of course, this condition differs from that in an immunocompetent patient, in which tumor development is modulated by the presence of an active immune system. Secondly, manipulation of cell lines prior to xenografting may modify the original pathogenic features of the tumor or lead to additional genetic defects. Moreover, neuroendocrine features of neuroblastoma cells limit successful subcutaneous implantation. Even if the injected cells resemble neuroblastoma *in situ*, it may be difficult to assess the exact stage of tumorigenesis. Finally, different commercial neuroblastoma cell lines display different properties in terms of malignancy and metastatic activity.

The above-mentioned biological features limit the possibility of obtaining a standardized murine model that allows assessment of neuroblastoma development and the response to pharmacological or genetic interventions. To overcome these limitations, Weiss and colleagues have generated a transgenic mouse model that spontaneously develops neuroblastoma with a phenotype very similar to the human disease (TH-MYCN mice) [10]. These mice are characterized by mis-expression of the human MYCN oncogene in neural-crest-derived cells, driven by the rat tyrosine hydroxylase promoter, leading to the accumulation of MYCN and to formation of tumors exclusively in the sympathoadrenal system. This model accurately reproduces the typical features of human neuroblastoma not only at the pathological level [11] but also in terms of genetic modifications [12–14] and microRNA expression profile [15].

Notwithstanding the advantages of this murine model, its potential has not been fully investigated due to the lack of tools available to non-invasively assess tumor presence and progression. In fact, arising in the murine abdomen, the tumor is not detectable until it achieves a size sufficient to be recognized through palpation of the mouse abdomen. In most cases, tumor progression is indirectly monitored by animal survival or by measuring tumor size by palpation of the abdomen [11, 16]. However, these methods are not accurate and require a large number of animals, whose generation and handling is both time-consuming and cost-intensive. Moreover, the operator experience is a crucial factor that strongly affects these measurements leading to inaccurate estimates of tumor size or failure to detect tumors at early disease stages.

Small animal PET (SA-PET) is a modern imaging technology that allows non-invasive analysis of tumor metabolism over time. Tumor behavior can be followed in small animals such as mice or rats, similarly as in a human patient in a clinical setting. Thanks to their good sensitivity and spatial resolution (approximately 1–1.5 mm) [17, 18], SA-PET tomographs can detect tumors at an early stage of development. Moreover, the possibility to sequentially perform imaging over time in the same animal further strengthens the results [19]. From a biological point of view, the non-invasive evaluation of tumor development from its early stages offers several advantages, particularly for drug testing studies, since the effect of a potential anti-tumor drug is better assessed in a small and well-vascularized mass without necrosis. The aim of the present study is to evaluate the potential of [^{18}F]FDG-SA-PET to monitor neuroblastoma development in transgenic TH-MYCN mice, in order to establish whether this imaging approach can be used as an accurate, reproducible, and non-invasive method to study disease evolution.

Materials and Methods

Study Design

SA-PET scans were performed in two cohorts of TH-MYCN homozygous animals. The first cohort (N = 39) was serially scanned over time at fixed intervals of time. SA-PET imaging was performed at day 0 in 30-day-old mice and repeated every 4 days until the 58th day of life. At the end of the monitoring period, animals were sacrificed and autoptic and pathologic examination was performed in order to confirm SA-PET findings.

A second group of animals (N = 25) was used to compare imaging data with *ex vivo* analysis of tumor volume and pathologic examination. In this case, animals were analyzed as above, but immediately sacrificed after the PET scan documenting the presence of viable tumor (first PET positive scan), or at the second, third, fourth, and fifth PET positive scan (N = 5 per each time point). Previous data obtained in our laboratory (data not shown) indicate that after the fifth positive PET scan (20 days after the first tumor detection), the tumor mass invades most of the abdomen and becomes indistinguishable from the physiologic uptake of abdominal organs. Therefore, we decided not to monitor tumor growth after this time point. Tumor volumes were estimated using the following formula: [(greatest diameter)×(smallest diameter)2]/2 [20].

TH-MYCN Mice

TH-MYCN homozygous mice (129X1/SvJ background) were obtained by backcrossing TH-MYCN hemizygous mice. All the experiments were reviewed and approved by the Bioethical Veterinary Committee of University of Bologna, Italy and by the Italian Ministry of Health (protocols 1237/P, 46903-X/6, and 20600-X/10). Animals were kept under pathogen-free conditions, with *ad libitum* access to food and water. Genomic DNA was isolated from mouse-tail tips from 17-day-old animals, and the genotype was determined by real-time quantitative PCR analysis using primers RBBI2 (533) s (CCTCTGCTAACCATGTTCA), MYCN (−128) as (ACAGC TCAAACACAGACAGAT) and as housekeeping mPOLR2DI1 (1151)s (CAGTTGCCAGGTGGATCTCTT), mPOLRD2DI1 (1287) as (TGCTCATGCCCACAATTAGTT). qPCR analysis was performed to quantify human MYCN transgene amplification using LightCycler®480 Roche, according to the manufacture's instruction and SYBR Green I Master (Roche Applied Science, Mannheim, Germany). PCR reaction conditions were 2 min at 50 °C and 10 min at 95 °C, for 50 cycles: 15 s at 95 °C and 60 s at 60 °C. The dosage of transgene in the samples was determined using the ΔC_t method, where the housekeeping gene was mPol and the calibrators were the parents' MYCN gene level.

SA-PET Imaging

SA-PET scans were carried out in all animals under sevofluorane (5 %) anesthesia (VetEquip System, Pleasanton, CA, USA) and oxygen supplementation (1 l/min). Each animal was injected with 15 MBq of [^{18}F]FDG in the tail vein (injected volume <0.15 ml) and scans started 60 min after tracer injection. After injection, animals were placed in a thermoregulated room (+22 °C) without anesthesia administration. The residual dose in the syringe was measured to verify the effective dose injected. PET image acquisition was performed using a small animal PET tomograph (GE eXplore Vista DR, Ontario, CA, USA) with a total acquisition time of 15 min. Since the axial field of view was 4 cm, a single bed position was sufficient to cover the whole animal body. Once the scan was completed, the animal was allowed to awake in a warmed recovery box.

Image Analysis

SA-PET images were reconstructed iteratively (OSEM 2D software) and red in three planes (axial, sagittal, coronal). Tumor metabolism was evaluated using semiquantitative analysis: Mean and maximum standard uptake values (SUV_{mean} and SUV_{max}, respectively) were calculated as the ratio of mean or maximum value of tissue radioactivity concentration (in millibecquerel per milliliter), respectively, and the injected dose (in millibecquerel), divided by the animal body weight. A volumetric region of interest was delineated in order to encompass the entire tumor lesion when an area of increased non-physiological tracer uptake was observed in a region of the abdomen located between the kidneys and the spine. When small tumor masses are analyzed, mean and maximum values of counts measured inside the tumor volume may be hampered by partial volume effect. In the light of the small size of the tumors detected by SA-PET in this murine model (see “Results” section), we used a partial volume effect correction method based on recovery coefficients (RC). As previously described by Aide et al [21], RC were determined using a phantom containing spheres with volumes ranging from 0.1 to 1.0 cc. RC values were plotted with respect to the spheres volume, and data were fitted using a sigmoid function [22, 23]. Correlation coefficients of fit were equal to 0.97 and 0.94, for RC curves calculated using maximum and mean value of counts, respectively. For each tumor size, RC values were calculated, using the plotted sigmoid function, and subsequently applied to correct both the SUV_{max} and the SUV_{mean} values.

Response to Chemotherapy Monitoring

Three TH-MYCN homozygous mice were evaluated by repeated SA-PET scans, following repeated treatment with chemotherapeutic agents currently used in clinical protocols against neuroblastoma [24]. Treatments started immediately after the first positive PET detection (first PET positive scan) in mouse 3, after the third PET positive scan in mouse 2, and after the fifth PET positive scan in mouse 1.

Mice received treatment by i.p. injection according to the following schedule: Carboplatin (30 mg/kg), vincristine (0.06 mg/kg), and etoposide (14 mg/kg) were injected in combination at days 1, 8, and 15; vincristine (0.12 mg/kg) and cisplatin (3.2 mg/kg) were injected in combination at days 4, 11, and 18. Carboplatin, vincristine, and cisplatin were purchased from BAXTER and etoposide from EBEWE.

In order to analyze chemotherapy-induced modifications in tumor SUVs, tumor volumes were estimated from PET images as described [25, 26]. Partial volume correction was applied in drug-treated mice as indicated in the “Image Analysis” section. In order to validate the method of tumor volume estimation in TH-MYCN mice, the size of tumors measured at sacrifice (collected *ex vivo*) were compared to estimated tumor size from the PET images obtained just prior to sacrifice.

Histology and Immunohistochemistry

All murine neuroblastomas were resected, measured, and fixed in 4 % formalin, dehydrated, embedded in paraffin, cut into 4-μm sections, and stained with hematoxylin and eosin (H&E) or processed for immunohistochemistry with a monoclonal anti-N-Myc primary antibody (Oncogene).

Statistical Analysis

The correlation between tumor [^{18}F]FDG uptake and human MYCN transgene amount was analyzed by the nonparametric Spearman rank test. Statistical analysis was performed with the software Prism Graphpad (Graphpad Prism v5.00, San Diego, CA, USA). P value<0.05 was considered statistically significant.

Results

Tumor Detection by SA-PET Imaging in TH-MYCN Homozygous Mice

SA-PET serial examination in 30-day-old TH-MYCN mice revealed the presence of abdominal areas of non-physiologic tracer uptake in 95 % of the mice studied (37 of 39 animals). Autopsy examination performed at the end of the experimental phase confirmed the presence of a single paraspinal mass, located between the kidneys, in 100 % of PET positive cases. In the advanced stages of tumor evolution, the mass adhered to surrounding organs and showed the presence of necrotic tissue. We did not see other areas of nonphysiological tracer uptake in all the mice analyzed, and these data were confirmed by the absence of metastases during autopsy. Figure 1 shows a representative SA-PET image of a transgenic homozygous mouse positive for neuroblastoma and the corresponding *ex vivo* appearance of the tumor mass.

Hematoxylin/eosin staining confirmed the presence of neuroblastoma in the [^{18}F]FDG avid lesions detected by SA-PET. In fact, small round blue cells were mixed with ganglionic-like differentiated elements (Figs. 1d and 2).

Only one of the two PET negative cases showed a small-sized paravertebral tumor lesion, while the other case was tumor free. As shown in Fig. 1e, 5.4 % of the animals was already positive at the early PET exam (30th day of life) and tumor prevalence progressively increased until the 46th day of life. Interestingly, the highest incidence of tumor occurrence was observed in a narrow range of time (ranging from the 34th to the 46th day of life), with an evident peak at day 34 (approximately 60 %). After this time point, no new cases were identified.

Analysis of Neuroblastoma Progression by SA-PET Imaging

SA-PET image analysis revealed a similar trend of tumor progression in almost all the PET-positive TH-MYCN mice analyzed (36 of 37 animals): The tumor mass was [^{18}F]FDG avid and showed a subsequent trend of rapidly increasing metabolic activity. In all these cases at the time of the fifth PET-positive scan, the tumor occupied an extended region of the mouse abdomen (Fig. 2).

The comparison of serial imaging data with *ex vivo* analysis of tumor volume and pathological features showed that the increase in [^{18}F]FDG uptake was paralleled by an increase in tumor size (Figs. 2 and 3a) and in modifications of the histological features of the tumor (Fig. 2). In the earliest stage of tumor development detected by SA-PET, necropsy and H&E analysis revealed the presence of a small and not vascularized tumor mass. We hypothesize that tumors arise from paraspinal or mesenteric ganglia because we observed

healthy medullas (data not shown) and the presence of ganglionic cells (Fig. 2) in several samples at the earliest stage.

The tumor mass appeared white in the first two stages and became progressively red in the next stages indicating a progression in the angiogenic processes (Fig. 2). The amount of necrosis, bleeding, and blood vessels increased from the second to the last positive scan.

N-Myc protein evaluated by immunohistochemistry was present at high levels in all stages (Fig. 2). The majority of cells in the samples were positive for the presence of nuclear N-Myc (Fig. 2). Kidney compartments were healthy and not infiltrated (data not shown). The tumor volume increased along the five different stages of PET positivity (Figs. 2 and 3a).

Interestingly, one of the 37 positive animals exhibited a clear arrest in tumor growth after the second PET positive scan. In this case, the [^{18}F]FDG signal disappeared at the third PET positive scan, and autopsy exam did not reveal any sign of a paraspinal mass. It is interesting in this regard that neuroblastoma in children shows the highest rate of spontaneous regression of any cancer [27]. Importantly, PET allowed the detection of very small abdominal tumors: In the animals with the earliest tumor occurrence detected by SA-PET, the mean tumor volume calculated *ex vivo* was 3.8 mm^3 (Figs. 2 and 3a).

To assess whether the increase in tumor size was accompanied by a modification of metabolic activity, we analyzed the variations of SUV_{mean} and SUV_{max} over time. Partial volume corrected analysis (Fig. 3b) of the parameter SUV_{mean} revealed that the metabolic activity of the tumor progressively increased during the first three time points reaching a plateau at the fourth and fifth positive PET scan (Fig. 3c). Accordingly, partial volume corrected analysis of the SUV_{max} (Fig. 3b) showed a similar trend (Fig. 3d). Intriguingly, both SUV_{mean} and SUV_{max} correlated with the human MYCN cDNA transgene levels measured in 17-day-old animals (when animal genotype was determined) (Fig. 4).

Analysis of Chemotherapy-Induced Tumor Regression by SA-PET Imaging

A group of three TH-MYCN homozygous animals treated with agents used in clinical protocols against neuroblastoma were studied by repeated [^{18}F]FDG -SA-PET scans. Previous experiments in our laboratory have shown that the chemotherapeutic drug combination used is effective in inducing tumor regression in TH-MYCN mice (data not shown).

In order to correct SUVs for partial volume effect, tumor volumes have been estimated from PET images in this group of mice [25, 26]. PET-based analysis of neuroblastoma volume is an accurate approach in TH-MYCN mice. Indeed, *ex vivo* analysis of tumor volumes is comparable with the tumor volume values estimated from the PET images during the five time points of PET positivity (supplementary Fig. 1).

As shown in Fig. 5 and Table 1, partial volume corrected SUV analysis of [^{18}F]FDG-SA-PET images revealed a clear and gradual reduction of the tumor metabolic activity during chemotherapy treatment, evident in all the three mice analyzed. Strikingly, 18 days of chemotherapy treatment completely eliminated tumor detection and image quantification in the first and the third PET-positive mouse (mice 2 and 3, respectively). Chemotherapy also modified [^{18}F]FDG uptake in the neuroblastoma lesion of the fifth PET positive mouse (mouse 1). In this case, however, the drugs treatment did not completely abrogate the PET signal. Necropsy performed at the end of the last PET imaging session (after 18 days of chemotherapy treatment) confirmed the imaging results. Indeed, no paraspinal masses were observed in mouse 2 and mouse 3, whereas a 750-mm^3 paraspinal mass was observed in mouse 1.

Discussion

Animal models of cancer accurately reflecting the biological and pathological features of human tumors are critical for development of novel therapies. To establish an ideal setting for testing new drugs, it is equally critical to detect tumors at early stages of development, when tumor masses are small, well-vascularized, and without necrosis. Moreover, from an experimental point of view, it is crucial to monitor tumor development over time, in order to detect drug-induced modification in the number of viable tumor cells and to assay for specific genetic alterations occurring later in the course of the disease.

Orthotopic or heterotopic rodent xenograft models are widely used animal models to study neuroblastoma. To explore the role of the proto-oncogene MYCN in neuroblastoma, a transgenic mouse model was created in which the MYCN oncogene was targeted to neuroectodermal cells of developing mice creating mice that overexpress MYCN in neural crest derived cells (TH-MYCN mice) [10]. As a transgenic model, TH-MYCN mice offer several advantages over xenografts models of neuroblastoma. Tumors develop spontaneously in TH-MYCN mice and show many of the pathogenetic features of human neuroblastoma. Indeed, comparative genomic hybridization has identified recurrent regions of chromosomal losses and gains that are syntenic with chromosomal aberrations in human neuroblastoma [10, 13, 14]. Moreover, as recently shown [11], these tumors display similar pathological features as the human neuroblastoma lesions. Furthermore, in contrast with xenograft models, where neuroblastoma develops in immunocompromised animals, neuroblastoma progression in TH-MYCN mice occurs in the presence of an intact immune system, thereby reflecting the human condition.

Conventionally used methods to monitor neuroblastoma development in TH-MYCN mice show poor accuracy, limiting the potential of this murine model. For example, palpation is frequently employed to detect tumors in these mice. This approach is hampered by several limitations. First, palpation only detects well advanced cases; furthermore, palpation is operator-dependent, cannot be considered suitable for serial measures over time (e.g., in drug testing studies), and does not provide information on the metabolic activity of the tumor.

Ex vivo analysis of the pathological features of the tumors obviously requires animal sacrifice with the consequent increase of both the number of animals needed to obtain definitive results and the total cost of the experiments. Therefore, non-invasive methodologies to detect neuroblastoma and to monitor changes in tumor metabolism over time represent important tools to fully exploit the potential of TH-MYCN mice. Pre-clinical imaging modalities, such as magnetic resonance imaging and optical imaging, have been recently proposed for the evaluation of TH-MYCN mice [28]. These procedures allow *in vivo* monitoring of tumor growth, but only provide anatomical information.

In vivo metabolic imaging of neuroblastoma in TH-MYCN mice has been reported using single-photon imaging combined with a large area detector [29]. This approach, however, is characterized by low-resolution and high-image noise, preventing the identification of tumors at early time points and limiting the ability to follow tumor progression over the time. High-resolution small animal PET scanners represent key tools to study anti-cancer drug efficacy in the pre-clinical setting. The great advantage of SA-PET over other molecular imaging techniques is to detect and semi-quantify the metabolic activity of the neoplastic lesion and to measure all metabolic changes of the mass over time. The aim of this study was to evaluate whether [^{18}F] FDG-SA-PET represents a useful imaging modality to non-invasively assess tumor presence and to monitor tumor development and metabolic activity in TH-MYCN mice.

To our knowledge, this is the first work describing the use of SA-PET in the TH-MYCN murine model. Our data show that [^{18}F]FDG-SA-PET can be effectively used to detect early developing neuroblastoma lesions and to monitor tumor metabolic changes over time. The tumor was [^{18}F]FDG avid and SA-PET detected spontaneously growing neuroblastoma in almost 100 % of TH-MYCN mice. Moreover, neuroblastoma lesions could be detected at a very early stage of their development. Indeed, by analyzing TH-MYCN mice by serial PET scans, it was possible to detect new positive cases with a mean tumor volume of 3.8 mm^3. It is also worth noticing that a high percentage of new positive cases could be detected in a narrow range of time, *i.e.*, between the 34th and 48th day of life. This important information will enable us to schedule future SA-PET imaging studies in a time window characterized by a very high probability to detect new born tumors in these transgenic mice.

Of note, SA-PET imaging detected a positive tumor in one TH-MYCN mouse that tended to disappear in the subsequent scans. This observation suggests that [^{18}F] FDG-SA-PET imaging can also be a useful tool to investigate the rare and recently documented [28] phenomenon of neuroblastoma regression in TH-MYCN mice. Understanding the regression process *in vivo* could help identifying the biological pathways that facilitate tumor growth arrest and lead to complete tumor regression.

We did not observe distant metastases during pathological examination of TH-MYCN mice. This finding, which is in contrast with the presence of gross liver, lung, and ovary metastases found by Weiss et al. in the same murine model [10], may be related to the background strain used (Weiss used Balb/c, C57B6/J, and FVB/N strains, while we used the 129X1/SvJ strain).

Our data also showed that SUV_{max} and SUV_{mean} parameters correlate with the human MYCN transgene genomic levels. Since disease severity is strictly dependent on the level of MYCN amplification in this transgenic model [10, 30, 31], this observation indicates that SUV measure reflects tumor malignancy. Moreover, these data highlight the potential of [^{18}F]FDG-SA-PET imaging for the non-invasive screening of new pharmacological approaches against neuroblastoma, acting as modulators of MYCN function.

The high uptake of [^{18}F]FDG that we observed in the *MYCN*-amplified TH-*MYCN* murine neuroblastomas clearly indicates avidity of these tumors for glucose. These data are in line with the essential role of MYCN in the Warburg effect (aerobic glycolysis requiring elevated glucose levels) in neuroblastomas, by upregulating multiple glycolytic genes [32, 33].

To provide additional evidence that [^{18}F]FDG-SA-PET is an effective tool for developmental therapeutics in neuroblastoma, we analyzed the time course of [^{18}F]FDG accumulation in TH-*MYCN* mice undergoing chemotherapy with drugs currently used for neuroblastoma treatment. SA-PET imaging provided information on drug-induced regression of tumor metabolic activity, highlighting the potential of this approach to assess neuroblastoma in TH-MYCN mice. Remarkably, the chemotherapy protocol led to elimination of tumor metabolic signals only in mice receiving treatment after the first and third PET scan indicating positivity. In the tumor treated at a later stage (after the fifth positive PET scan), chemotherapy led to a reduction of signal, without complete cessation. These results reflect clinical scenarios, in which chemotherapy is unable to cure MYCN-driven neuroblastomas, and suggest early detection and early initiation of treatment as critical for a positive outcome in high-risk, MYCN-amplified neuroblastoma.

Altogether, these data indicate that [^{18}F]FDG-SA-PET imaging is a valid tool to non-invasively detect spontaneously growing neuroblastoma in TH-MYCN transgenic mice.

Future studies with this non-invasive approach will allow to better exploit the full potential of this important preclinical model of neuroblastoma.

Supplementary Material

Refer to Web version on PubMed Central for supplementary material.

Acknowledgments

We thank Dr. Pasquale Chieco and the Center for Applied Biomedical Research (CRBA), S. Orsola-Malpighi University Hospital, Via Massarenti 9, 40138 Bologna, Italy for support and expert assistance with histology and immunohistochemistry. We thank Prof. Hein te Riele for editorial and scientific suggestions. We thank the Italian Foundation for Neuroblastoma Research, AIRC, AGEOP, and NIH R01CA102321 for support.

References

1. Brodeur GM. Neuroblastoma: biological insights into a clinical enigma. Nat Rev Cancer. 2003; 3:203–216. [PubMed: 12612655]
2. Howman-Giles R, Shaw PJ, Uren RF, et al. Neuroblastoma and other neuroendocrine tumors. Semin Nucl Med. 2007; 37:286–302. [PubMed: 17544628]
3. Kushner BH. Neuroblastoma: a disease requiring a multitude of imaging studies. J Nucl Med. 2004; 45:1172–1188. [PubMed: 15235064]
4. Melzer HI, Coppenrath E, Schmid I, et al. 333I-MIBG scintigraphy/SPECT versus ^{18}F-FDG PET in paediatric neuroblastoma. Eur J Nucl Med Mol Imaging. 2011; 38:1648–1658. [PubMed: 21617976]
5. Sharp SE, Shulkin BL, Gelfand MJ, et al. 123I-MIBG scintigraphy and ^{18}F-FDG PET in neuroblastoma. J Nucl Med. 2009; 50:1237–1243. [PubMed: 19617326]
6. Papathanasiou ND, Gaze MN, Sullivan K, et al. ^{18}F-FDG PET/CT and 123I-metaiodobenzylguanidine imaging in high-risk neuroblastoma: diagnostic comparison and survival analysis. J Nucl Med. 2011; 52:519–525. [PubMed: 21421719]
7. Franzius C. FDG-PET/CT in pediatric solid tumors. Q J Nucl Med Mol Imaging. 2010; 54:401–410. [PubMed: 20823808]
8. Piccardo A, Lopci E, Conte M, et al. Comparison of ^{18}F-dopa PET/CT and 123I-MIBG scintigraphy in stage 3 and 4 neuroblastoma: a pilot study. Eur J Nucl Med Mol Imaging. 2012; 39:57–71. [PubMed: 21932116]
9. Kroiss A, Putzer D, Uprimny C, Decristoforo C, et al. Functional imaging in phaeochromocytoma and neuroblastoma with 68 Ga-DOTA-Tyr 3-octreotide positron emission tomography and 123I-metaiodoben-zylguanidine. Eur J Nucl Med Mol Imaging. 2011; 38:865–873. [PubMed: 21279352]
10. Weiss WA, Aldape K, Mohapatra G, Feuerstein BG, Bishop JM. Targeted expression of MYCN causes neuroblastoma in transgenic mice. EMBO J. 1997; 16:2985–2995. [PubMed: 9214616]
11. Moore HC, Wood KM, Jackson MS, et al. Histological profile of tumors from MYCN transgenic mice. J Clin Pathol. 2008; 61:1098–1103. [PubMed: 18682419]
12. Weiss WA, Godfrey T, Francisco C, Bishop JM. Genome-wide screen for allelic imbalance in a mouse model for neuroblastoma. Cancer Res. 2000; 609:2483–2487. [PubMed: 10811128]
13. Hackett CS, Hodgson JG, Law ME, et al. Genomewide array CGH analysis of murine neuroblastoma reveals distinct genomic aberrations which parallel those in human tumors. Cancer Res. 2003; 6317:5266–5273. [PubMed: 14500357]
14. Norris MD, Burkhart CA, Marshall GM, Weiss WA, Haber M. Expression of N-myc and MRP genes and their relationship to N-myc gene dosage and tumor formation in a murine neuroblastoma model. Med Pediatr Oncol. 2000; 356:585–589. [PubMed: 11107123]
15. Terrile M, Bryan K, Vaughan L, et al. miRNA expression profiling of the murine TH-MYCN neuroblastoma model reveals similarities with human tumors and identifies novel candidate miRNAs. PLoS One. 2011; 6:e28356. [PubMed: 22164278]

16. Chesler L, Goldenberg DD, Seales IT, et al. Malignant progression and blockade of angiogenesis in a murine transgenic model of neuroblastoma. Cancer Res. 2007; 67:9435–9442. [PubMed: 17909053]

17. Tai YC, Ruangma A, Rowland D, et al. Performance evaluation of the microPET focus: a third generation microPET scanner dedicated to animal imaging. J Nucl Med. 2005; 46:455–463. [PubMed: 15750159]

18. Spinelli AE, D'Ambrosio D, Pettinato C, et al. Performance evaluation of a small animal PET scanner. Spatial resolution characterization using 18F and 11C. Nucl Inst Methods Phys Res A. 2007; 571:215–218.

19. Wang J, Maurer L. Positron emission tomography: applications in drug discovery and drug development. Curr Top Med Chem. 2005; 5:1053–1075. [PubMed: 16181131]

20. Hwang RF, Yokoi K, Bucana CD, et al. Inhibition of platelet-derived growth factor receptor phosphorylation by STI571 (Gleevec) reduces growth and metastasis of human pancreatic carcinoma in an orthotopic nude mouse model. Clin Cancer Res. 2003; 9:6534–6544. [PubMed: 14695158]

21. Aide N, Louis MH, Dutoit S, et al. Improvement of semi-quantitative small-animal PET data with recovery coefficients: a phantom and rat study. Nucl Med Commun. 2007; 28:813–822. [PubMed: 17728612]

22. Hoffman EJ, Huang SC, Phelps ME. Quantitation in positron emission computed tomography: 1. Effect of object size. J Comput Assist Tomogr. 1979; 3:299–308. [PubMed: 438372]

23. Zhang H, Inoue T, Alyafei S, et al. Tumor detectability in 2-dimensional and 3-dimensional positron emission tomography using the SET-2400W: a phantom study. Nucl Med Commun. 2001; 22:305–314. [PubMed: 11314763]

24. Ladenstein R, Valteau-Couanet D, Brock P, et al. Randomized trial of prophylactic granulocyte colony-stimulating factor during rapid COJEC induction in pediatric patients with high-risk neuroblastoma: the European HR-NBL1/SIOPEN study. J Clin Oncol. 2010; 21:3516–3524. [PubMed: 20567002]

25. Tylski P, Stute S, Grotus N, et al. Comparative assessment of methods for estimating tumor volume and standardized uptake value in 18F-FDG PET. J Nucl Med. 2010; 51:268–276. [PubMed: 20080896]

26. Nestle U, Kremp S, Schaefer-Schuler A, et al. Comparison of different methods for delineation of ^{18}F-FDG PET-positive tissue for target volume definition in radiotherapy of patients with non-small cell lung cancer. J Nucl Med. 2005; 46:1342–1348. [PubMed: 16085592]

27. Maris JM. Recent advances in neuroblastoma. N Engl J Med. 2010; 36223:2202–2211. [PubMed: 20558371]

28. Teitz T, Stanke JJ, Federico S, et al. Preclinical models for neuroblastoma: establishing a baseline for treatment. PLoS One. 2011; 29(6):e19133. [PubMed: 21559450]

29. Accorsi R, Morowitz MJ, Charron M, et al. Pinhole imaging of 131I-metaiodobenzylguanidine (131I-MIBG) in an animal model of neuroblastoma. Pediatr Radiol. 2003; 33:688–692. [PubMed: 12908090]

30. Hackett CS, Hodgson JG, Law ME, et al. Genome-wide array CGH analysis of murine neuroblastoma reveals distinct genomic aberrations which parallel those in human tumors. Cancer Res. 2003; 17:5266–5273. [PubMed: 14500357]

31. Hansford LM, Thomas WD, Keating JM, et al. Mechanisms of embryonal tumor initiation: distinct roles for MycN expression and MYCN amplification. Proc Natl Acad Sci U S A. 2004; 101:12664–12669. [PubMed: 15314226]

32. Qing G, Skuli N, Mayes PA, et al. Combinatorial regulation of neuroblastoma tumor progression by N-Myc and hypoxia inducible factor HIF-1alpha. Cancer Res. 2010 Dec 15; 70(24):10351–10361. [PubMed: 20961996]

33. Chen QR, Song YK, Yu LR, et al. Global genomic and proteomic analysis identifies biological pathways related to high-risk neuroblastoma. J Proteome Res. 2010 Jan.9:373–382. [PubMed: 19921788]

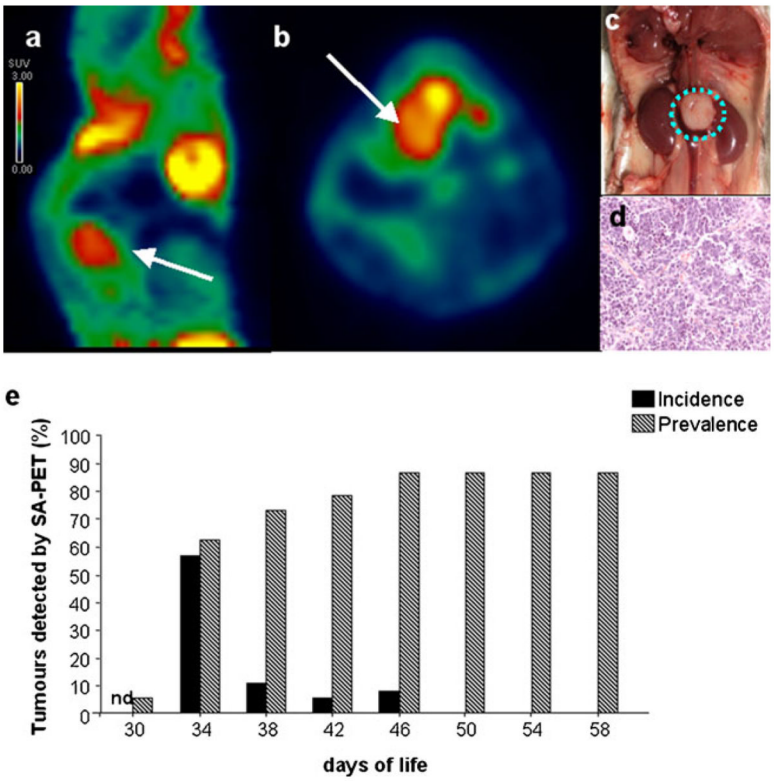

Fig. 1.

Neuroblastoma detection in TH-MYCN mice by SA-PET imaging. **a**, **b** SA-PET image (sagittal and axial view, respectively) showing a paraspinal neuroblastoma lesion in a TH-MYCN transgenic mouse. **c**, **d** Appearance of the tumor shown in **a** and **b** at autopsy and by H&E histology. In all the mice studied, a paraspinal neuroblastoma mass localized between the kidneys and H&E staining showed a sheet-like arrangement. **e** Percent incidence (newly detected tumors) and prevalence of neuroblastoma detected by SA-PET scan in TH-MYCN homozygous mice analyzed every 4 days ($n = 39$). *Nd* not determined.

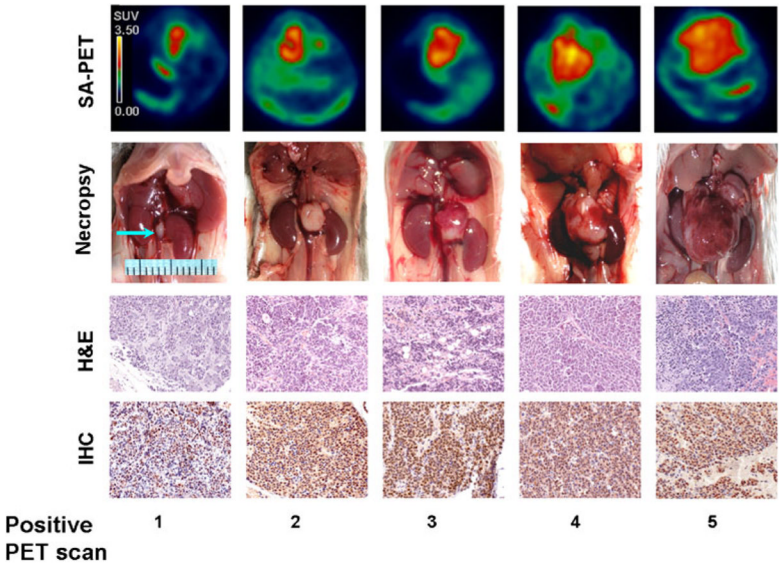

Fig. 2.

SA-PET and *ex vivo* analysis of tumor progression in TH-MYCN mice. Comparison between SA-PET and *ex vivo* analysis of tumor progression in TH-MYCN mice. SA-PET imaging (axial view), autopsy, H&E staining, and immunohistochemistry with monoclonal anti-N-Myc antibody (IHC) are shown in mice analyzed at five different stages of PET positivity. Radioactive counts in SA-PET images are expressed as SUV.

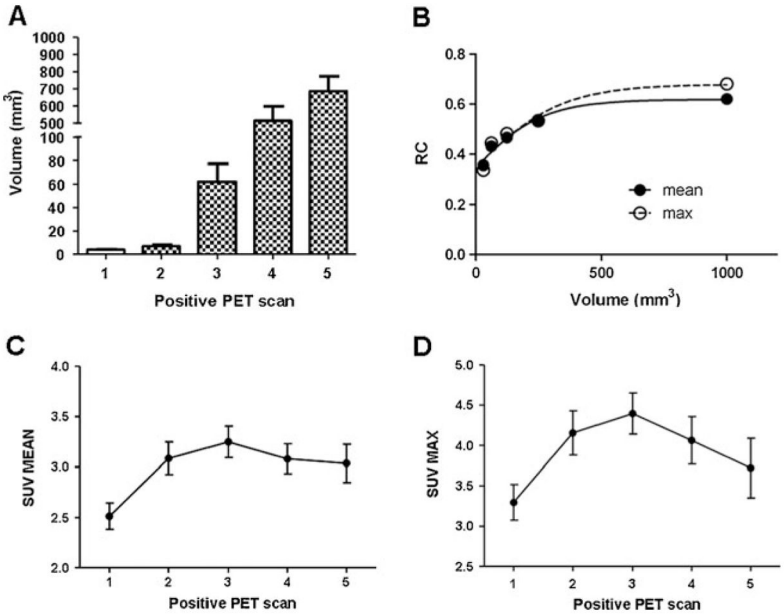

Fig. 3.

SA-PET analysis of tumor metabolism in TH-MYCN mice. **a** Tumor volumes calculated in TH-MYCN mice sacrificed at various time points of PET positivity. Data are expressed as mean±SEM. $N = 4–5$ for each time point. **b** Recovery coefficient (*RC*) values derived from SA-PET acquisition of radioactive spheres of several diameters. Data were fitted using a sigmoid function. **c** Analysis of SUV_{mean} in five different PET time points reflecting different stages of positivity. Values are expressed as mean±SEM. $N = 20–30$ for each time point. **d** Analysis of SUV_{max} in five different PET time points reflecting different stages of positivity. Values are expressed as mean±SEM. $N = 20–30$ for each time point.

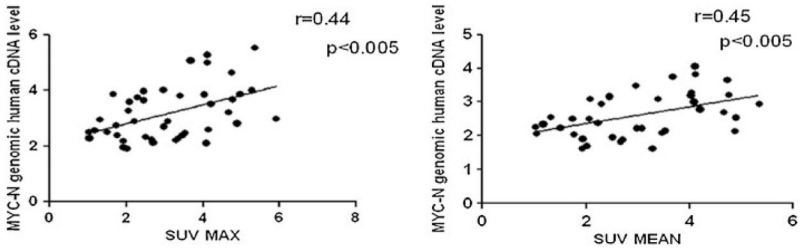

Fig. 4.

Correlation between SUV and MYCN transgene amount. Correlation between the human MYCN cDNA level and the SUV_{mean}, or the SUV_{max}, in TH-MYCN homozygous mice analyzed at different stages of PET positivity. Spearman *r* values and linear regression slope are shown on the graphs.

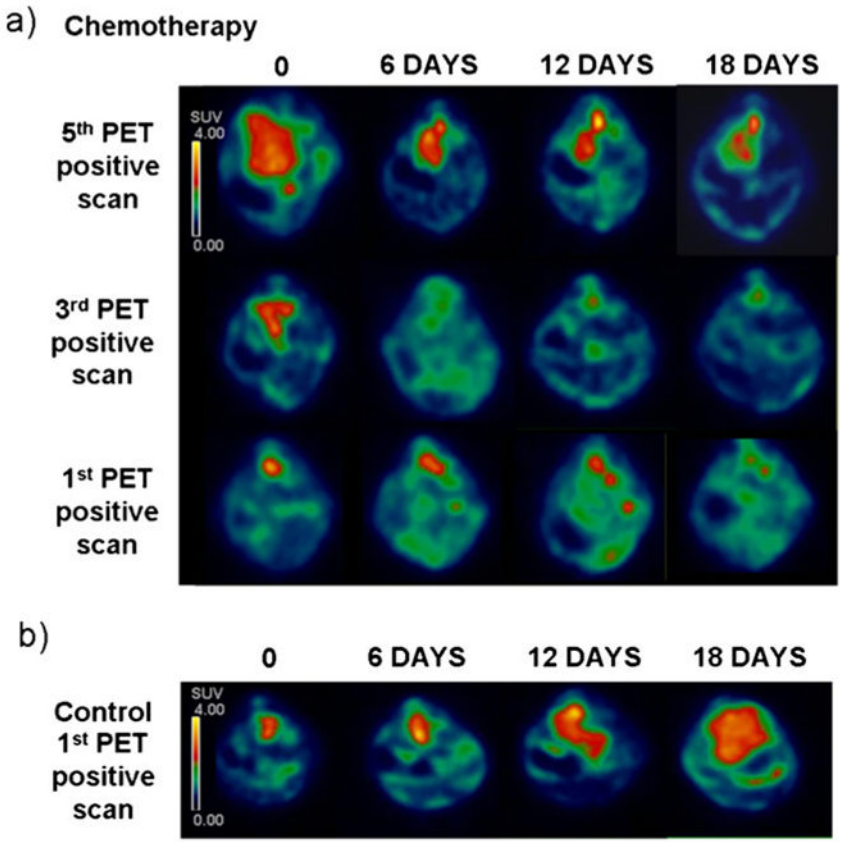

Fig. 5.

SA-PET analysis of tumor regression after chemotherapy treatment in TH-MYCN mice. **a** SA-PET images (axial view) of three TH-MYCN mice treated with a chemotherapy cocktail against neuroblastoma. Chemotherapy treatment started after the fifth PET positive scan in mouse 1 (*top*), after the third PET positive scan in mouse 2 (*middle*), and after the first PET positive scan in mouse 3 (*bottom*). SA-PET scanning has been repeated in these mice after 6, 12, and 18 days from the starting of chemotherapy. Radioactive counts are expressed as SUV. **b** Control TH-MYCN mouse analyzed by SA-PET images after 6, 12, and 18 days from the first PET positive scan. Radioactive counts are expressed as SUV.

Table 1

SUV_{mean} values corresponding to the SA-PET images shown in Fig. 5

Chemotherapy	SUV 1st PET positive scan	SUV 3rd PET positive scan	SUV 5th PET positive scan
0	3.2	3.9	3.5
6 days	2.4	ND	3.1
12 days	2	ND	4.2
18 days	ND	ND	3.4

ND not detectable